Journal of Nuclear Materials 618 (2026) 156228

Contents lists available at ScienceDirect

Journal of Nuclear Materials

journal homepage: www.elsevier.com/locate/jnucmat

Assessment of EUROFER97, tungsten and CuCrZr alloy transmutation effects under IFMIF-DONES and DEMO conditions

Irene Álvarez [a,b], Marta Anguiano [a,*], Fernando Mota [b], Rebeca Hernández [c], Marta Serrano [c], David Sosa [b], Iole Palermo [b], Edgar Leon-Gutierrez [b], Simone Noce [d], Fabio Moro [d], Frederik Arbeiter [e], Yuefeng Qiu [e], Jin Hun Park [e], Ángel Ibarra [b,f]

[a] Department of Atomic, Molecular and Nuclear Physics, University of Granada, UGR, Granada, Spain
[b] Laboratorio Nacional de Fusión, CIEMAT, Madrid, Spain
[c] División de Materiales de Interés energético, CIEMAT, Madrid, Spain
[d] Nuclear Department, ENEA Frascati, Rome, Italy
[e] Karlsruhe Institute of Technology, KIT, Karlsruhe, Germany
[f] IFMIF-DONES España, Granada, Spain

ARTICLE INFO

Keywords:
IFMIF-DONES
DEMO
Transmutation
Comparative

IFMIF-DONES (International Fusion Materials Irradiation Facility – DEMO-Oriented Neutron Source) is a specialised neutron irradiation facility designed to generate critical materials data needed for the construction of the DEMO (DEMOnstration) fusion power plant. This study aims to analyse and characterise the transmutation behaviour of materials such as EUROFER97, tungsten, and CuCrZr alloy under the IFMIF-DONES irradiation conditions and comparing them with the typical DEMO radiation field. Nominal IFMIF-DONES beam conditions and different DEMO concepts have been used allowing a comparison of the DEMO and IFMIF-DONES environments. From the results obtained, it can be concluded that the transmutation damage in EUROFER97, obtained in IFMIF-DONES, reproduces to a large extent what will occur in DEMO. However, large discrepancies have been observed in the specific location studied for the W and the CuCrZr alloy.

1. Introduction

The neutron irradiation conditions characterised by high-energy neutrons in the future nuclear fusion power plant DEMO present significant uncertainties regarding the evolution of material properties evolution throughout the reactor's operational lifetime. The mission of the International Fusion Materials Irradiation Facility – DEMO Oriented Neutron Source (IFMIF-DONES) [1,2] is to evaluate and qualify materials performance by subjecting them to realistic nuclear fusion irradiation conditions and doses comparable to those expected in the DEMO fusion power plant.

Primary displacement damage rate studies have been already carried out for IFMIF-DONES and for DEMO [3–5], so this study focuses on the case of transmutation at both facilities.

Transmutation is a type of damage that directly affects the material properties, making it crucial to compare transmutation in both IFMIF-DONES and DEMO. It is a process in which nuclear reactions alter the proportion of elements and isotopes in a material. This transformation can modify the chemical composition, mechanical properties, microstructure, and, in general, radiation resistance of structural materials, potentially causing embrittlement, swelling, or changes in thermal conductivity [6,7]. Among the materials to be considered in the EUROfusion roadmap are EUROFER97, tungsten, and CuCrZr alloy [8], so they are the materials chosen for this study.

The study of transmutation in IFMIF-DONES and DEMO is key issue to assess whether the transmutation rates and underlying physical mechanisms are comparable. Ensuring that IFMIF-DONES replicates transmutation effects similar to those expected in DEMO is essential for qualifying candidate materials under representative conditions, thus enabling reliable predictions of their long-term performance in future fusion reactors.

The core of the IFMIF-DONES facility is the Test Cell, where the High Flux Test Module (HFTM) is located, which will host the material specimens. To reproduce the nuclear fusion irradiation conditions, a deuteron beam (D^+) with a nominal energy of 40 MeV and 125 mA will impact with a lithium jet ($^{6,7}Li$), generating $6.8 \bullet 10^{16}$ neutrons/s [9].

* Corresponding author.
E-mail address: mangui@ugr.es (M. Anguiano).

https://doi.org/10.1016/j.jnucmat.2025.156228
Received 28 May 2025; Received in revised form 10 October 2025; Accepted 14 October 2025
Available online 15 October 2025

This reaction produces a neutron spectrum with a broad peak at 14 MeV and a maximum energy of up to 55 MeV (Fig. 2) [5].

In the frame of the EUROfusion roadmap, three breeders blanket concepts are considered for DEMO: the Dual Coolant Lithium Lead (DCLL) [10,11], the Water Cooled Lithium Lead (WCLL) [12–14], and the Helium Cooled Pebble Bed (HCPB) [15–17]. The neutron spectra in the first wall and divertor have been calculated for each one.

The following section presents the methodology, results, discussion, and conclusions. The results are organised by the materials studied. For each material, the results obtained for IFMIF-DONES — with a nominal deuteron beam energy of 40 MeV but adjustable down to 25 MeV [2] — are presented for these two extreme values of the operational range, and compared with those calculated for the different DEMO concepts.

2. Methodology

2.1. Tools used for neutron transport calculations

The specimen packaging of IFMIF-DONES HFTM used is the CLC.v2.0 model, described in [4]. For the calculation of transmutation in IFMIF-DONES, it has been considered the neutron spectrum of a tensile-type specimen in rig 45, in the first line of the beam (Fig. 1), from now specimen A. To model the IFMIF-DONES deuteron–lithium neutron source, neutron transport simulations were carried out with the McDeLicious code — a tool based on MCNP6.2 and developed by the Karlsruhe Institute of Technology (KIT) [18], using the FENDL.3.1d nuclear data library [19] and the Test Cell model mdl9.2.8 [20,21]. The IFMIF-EVEDA (International Fusion Materials Irradiation Facility - Engineering Validation and Engineering Design Activities) beam profile has been used in the standard footprint size 20×5 cm^2 and the deuteron energies 25 and 40 MeV (to cover the energy range of the accelerator), as commented above. The data have been obtained for the three considered materials.

In the case of IFMIF-DONES, two different cases are analysed: HFTM_20_25 and HFTM_20_40, for the 25 MeV and 40 MeV beam energies. HFTM indicates that the data come from IFMIF-DONES HFTM; the 20 from the beam footprint size used, and the last number corresponds to the beam energy.

In the case of DEMO, three different blanket concepts included in the EUROfusion roadmap have been considered: DCLL, WCLL and HCPB. The positions chosen are the first wall (FW) inboard at the equatorial level and the divertor area (DIV). The foreseen materials for the FW are EUROFER97 and W, while the DIV are W and CuCrZr alloy [22]. The fusion power for all the DEMO concepts is 1998 MW. The spectra for the WCLL concept were provided by the ENEA, those for the DCLL concept by the CIEMAT, and those for the HCPB concept by the KIT. A comparison of the different neutron spectra used for the isotopic inventory calculations is shown in Fig. 2, considering in all the cases 211 energy groups (VITMAIN-J+).

2.2. Studied materials

Among the materials included in the EUROfusion roadmap for the construction of DEMO, EUROFER97 [23–26], W [27,28] and the CuCrZr [29,30] alloy are of particular relevance [22,31]. Therefore, the degradation of their macroscopic properties will be assessed by irradiation experiments in the IFMIF-DONES facility, carried out in several campaigns under conditions representative of those expected in the future DEMO nuclear power plant. These studies aim to generate a comprehensive database of material behaviour to support the design and construction of DEMO.

EUROFER97 is a Reduced Activation Ferritic Martensitic (RAFM) steel developed for use in fusion reactors, particularly in the FW. It minimises swelling and helium production under neutron irradiation [22]. Its composition replaces highly activating elements (such as Mo, Nb and Ni) with Ta, W and V to reduce long-term radioactivity [32]. EUROFER97 also retains its magnetic and structural properties at high temperatures and in strong magnetic fields, making it well suited for fusion reactor operation [33].

W is being considered for use in DEMO FW and DIV to protect plasma-facing components [22,31]. This material is important in fusion due to its exceptionally high melting point (around 3400 °C), which allows it to withstand extreme temperatures. In addition, W is highly resistant to radiation [34], making it suitable for fusion environments. W also has excellent thermal conductivity, high resistance to plasma sputtering and low tritium retention, making it a reliable choice for demanding fusion applications [35,36].

The CuCrZr alloy will be used as the thermal interface, acting as a heat sink material in the DEMO DIV [22]. This alloy combines the excellent thermal and electrical conductivity of Cu, which effectively dissipates heat in the divertor, with the enhanced mechanical strength of the Cr and Zr addition [37,38]. These additions enhance the alloy's resistance to mechanical stress and thermal cycling, making it ideal for demanding applications. In addition, the alloy offers good ductility and corrosion resistance, ensuring durability and long life in the nuclear fusion environment [39–42].

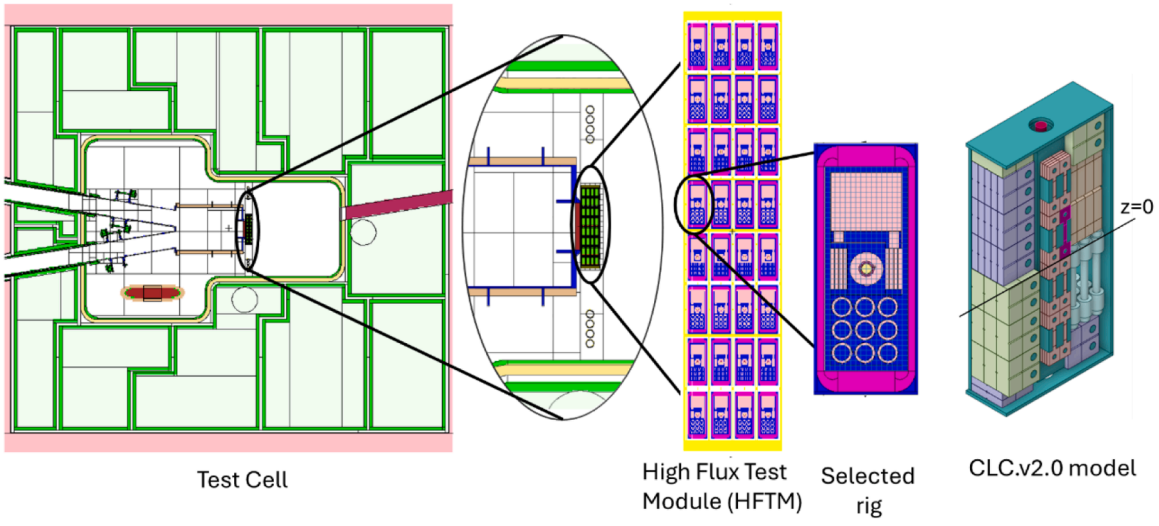

Fig. 1. Test Cell horizontal cross section at $z = 0$ with the CLC.v2.0 specimen distribution model in the HFTM. The selected rig is the 45, and the highlighted specimen is the one selected for the transmutation study, specimen A.

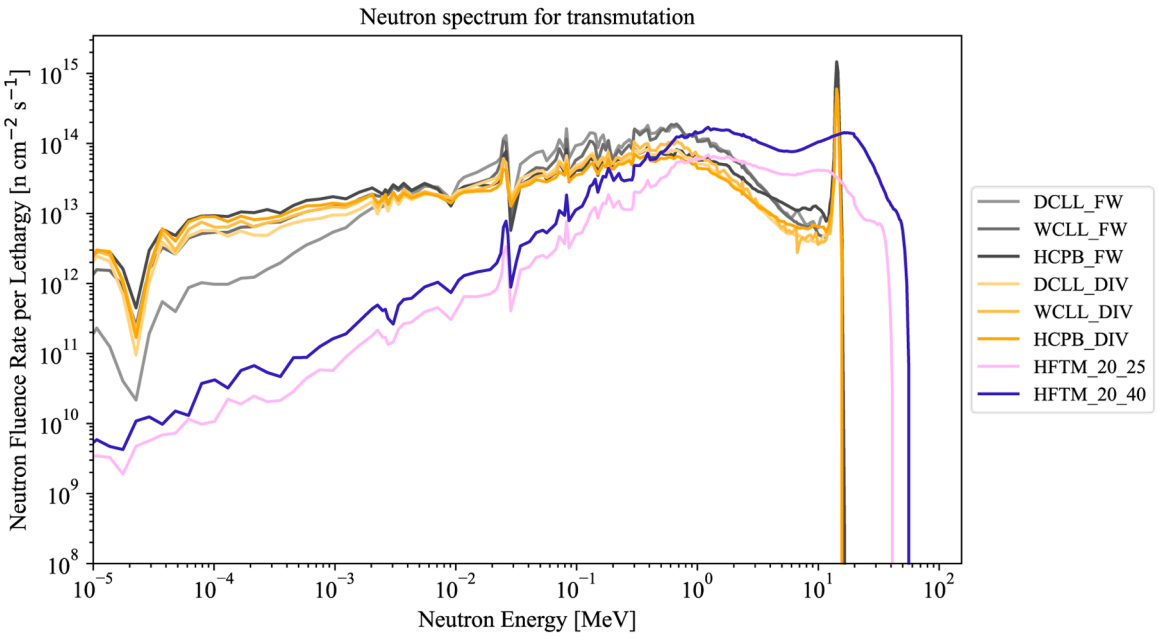

Fig. 2. Neutron fluence rate in the first wall and divertor of each DEMO concept, together with the neutron fluence rate obtained in the EUROFER97 tensile specimen A in rig 45 of HFTM.

The initial compositions of EUROFER97, W and CuCrZr alloy considered for the calculations are provided in Table 1. The atomic density EUROFER97 is 8.52•10^{22} atoms cm^{-3}, and its mass density is 7.87 g cm^{-3}. In the case of W, the atomic density is 6.24•10^{22} atoms cm^{-3} and the mass density is 19 g cm^{-3}. For the CuCrZr alloy, the atomic density and mass density are 8.46•10^{22} atoms cm^{-3} and 7.9 g cm^{-3}, respectively.

Table 1
Initial composition of EUROFER97, W and CuCrZr alloy [43,44].

	Weight percent [wt%]		
	EUROFER97	W	CuCrZr alloy
H		5.00•10^{-4}	
B	2.00•10^{-3}		6.00•10^{-3}
C	1.10•10^{-1}	3.00•10^{-3}	
N	3.00•10^{-2}	5.00•10^{-4}	
O	1.00•10^{-2}	2.00•10^{-3}	1.30•10^{-1}
Na		1.00•10^{-3}	
Mg		5.00•10^{-4}	1.00•10^{-1}
Al	1.00•10^{-2}	1.50•10^{-3}	7.00•10^{-3}
Si	5.00•10^{-2}	2.00•10^{-3}	9.00•10^{-2}
P	5.00•10^{-3}	2.00•10^{-3}	3.00•10^{-2}
S	5.00•10^{-3}	5.00•10^{-4}	8.00•10^{-3}
K		1.00•10^{-3}	
Ca		5.00•10^{-4}	
Ti	2.00•10^{-2}	5.00•10^{-4}	
V	2.00•10^{-1}		
Cr	9.01•10^{0}	2.00•10^{-3}	1.10•10^{0}
Mn	4.00•10^{-1}	5.00•10^{-4}	2.30•10^{-3}
Fe	8.87•10^{1}	3.00•10^{-3}	2.30•10^{-2}
Co	1.00•10^{-2}	1.00•10^{-3}	5.00•10^{-2}
Ni	1.00•10^{-2}	5.00•10^{-4}	7.00•10^{-2}
Cu	1.00•10^{-2}	1.00•10^{-3}	9.82•10^{1}
Zn		5.00•10^{-4}	5.00•10^{-3}
As		5.00•10^{-4}	9.00•10^{-3}
Zr	5.00•10^{-2}	5.00•10^{-4}	1.04•10^{-1}
Nb	5.00•10^{-3}	1.00•10^{-3}	6.80•10^{-2}
Mo	5.00•10^{-3}	1.00•10^{-2}	
Ag		1.00•10^{-3}	
Cd		5.00•10^{-4}	
Sn	5.00•10^{-2}		5.00E-03
Sb	5.00•10^{-2}		6.00E-03
Ta	1.20•10^{-1}	2.00•10^{-3}	4.00E-03
W	1.10•10^{0}	99.95•10^{0}	
Pb		5.00•10^{-4}	3.00•10^{-3}
Bi			1.00•10^{-3}
Ba		5.00•10^{-4}	
Total	1.00•10^{2}	1.00•10^{2}	1.00•10^{2}

2.3. Transmutation calculation methodology

The code used for the isotopic inventory calculations is ACAB [45]. The output data have been processed by ACABAN (Fortran code) and Python. The inputs of this code are the neutron spectra and the composition of the irradiated material. The nuclear data library used is TENDL2017 [46].

All the calculations have considered a full power year (fpy) of 365.25 days. The results are present in weight percent [wt%], which represents the concentration of an element in a material relative to its mass. It is calculated as presented in Eq. (1).

$$\text{wt\%} = \frac{\text{mass of the element}}{\text{total mass of the material}} 100. \quad (1)$$

Graphs will be presented in transmutation rate [%/fpy] and number of atoms in [appm/NRT_dpa]. The transmutation rate (TR) is a value that represents the quantity of atoms present in the material after irradiation with respect to the initial amount per element (Eq. (2)).

$$\text{TR}\left[\frac{\%}{\text{fpy}}\right] = \frac{\text{N° atoms after irradiation} - \text{Initial N° atoms}}{\text{Initial N° atoms}} 100. \quad (2)$$

The primary displacement damage rate allows the quantification of the accumulated primary displacement damage in the material; the measurement unit is displacement per atom (dpa). To obtain this magnitude it has been used the Norgett Robinson Torrens (NRT_dpa) [47] methodology in the Monte Carlo calculation as explained in [4,5]. These values have been calculated using the MCNP6.2 code [48] and the JEFF.3.3arc nuclear data library [49]. The primary displacement damage rate has been used as reference to obtain the atoms per dpa ratio. Therefore, the other parameter used is in atoms, parts per million [appm] units per primary displacement damage ratio [NRT_dpa] (Eq. (3)).

$$\text{Atoms per dpa}\left[\frac{\text{appm}}{\text{NRT\_dpa}}\right] = \frac{\dfrac{\text{isotope quantity}\left[\frac{\text{atoms}}{\text{cm}^3\ \text{fpy}}\right]}{\text{atomic density of the material}\left[\frac{\text{atoms}}{\text{cm}^3}\right]}10^6}{\text{Primary displacement damage rate}\left[\frac{\text{NRT\_dpa}}{\text{fpy}}\right]}. \quad (3)$$

In the case of EUROFER97, TR is used for the elements initially present in its composition and the Atoms per dpa for the new elements produced. For W and CuCrZr alloy only the Atoms per dpa parameter is used.

3. Results

This section presents the transmutation results calculated. It is divided into three sections, one per material studied.

The analysis presented supplies a global perspective on how the initial material composition changes after irradiation in IFMIF-DONES and DEMO. It focuses on the evolution of the elements originally present in the material as well as the formation of new elements generated by transmutation processes.

3.1. EUROFER97

In the case of the EUROFER97 transmutation, the elements that show the highest transmutation rate are Ti, V, Mn, and Ta, which are represented in Fig. 3 with a different scale, for them, the DEMO FW values obtained agree in the same range. Meanwhile, in the IFMIF-DONES specimen with 25 MeV beam energy, the values are well below the DEMO range, but at 40 MeV, the values are well above the DEMO range. In the Ta case, in DEMO FW it is consumed, while in the IFMIF-DONES specimen, it is generated, but in a minor quantity (Fig. 3).

Fig. 3 also shows the transmutation rate of the rest of the elements present initially in the EUROFER97 composition, (omitting the Ti, V, Mn and Ta). The calculated transmutation rate for DEMO is below 3 % in all cases, and for IFMIF-DONES it is in general below 1.5 %. The DEMO transmutation rate is practically the similar for the three DEMO designs, except for B, Sb, which is more burned up in the HCPB than in the DCLL case, and for Co, for the HCPB breeding blanket presents the highest generation. In the IFMIF-DONES case, it either generates or burns up, it will be higher the higher the energy beam is.

Table 2 presents the primary displacement damage rate induced for specimen A at different IFMIF-DONES beam energies, and the data corresponding to the FW of the different DEMO concepts [4]. The elements generated during the irradiation are presented in Fig. 4 as number of atoms generated per primary displacement damage rate [appm NRT_dpa^{-1}]. The primary displacement damage rate considered in each scenario is the presented in Table 2. As mentioned above, the number of atoms generated for each element increases with the IFMIF-DONES beam energy but normalizing to the NRT_dpa can be observed that the ratio is in good agreement when the element is generated. For the three DEMO concepts, the FW values remain practically the same for H, He, Be, Mg, Y, and Hf. On the other hand, Li, Te, Re, and Os have different values in the different DEMO cases, increasing from DCLL to HCPB. A special case is Os, which is not produced in IFMIF-DONES but is produced in the DEMO layouts.

Table 3 shows the initial EUROFER97 composition used in the calculation, together with the material specifications, as well as its final compositions after 1 fpy of irradiation for the five cases considered. In EUROFER97 there is a composition specification defined for the material, allowing for some range of tolerance in the elements present [44]. The table present the same data that the figures in a complete way. The new elements generated from the initial composition of EUROFER 97 are H, He, Li, Be, Mg, Y, Te, Hf, Re and Os. However, not in all cases these elements are generated, for example, Os is only generated in DEMO FW. Elements such as C, N, Al, Si, P, S, V, Cr, Mn, Fe, Mo, and W exhibit low variability and remain within acceptable composition limits, according to the specifications. Although the initial concentrations of B, Co, Nb, Ni, Cu, Zr, Sn, Sb, and Ta exceed the specified limits, their levels

Table 2
Primary displacement damage rate in [NRT_dpa fpy^{-1}] in the chosen specimen in IFMIF-DONES and in the first wall of DEMO in the case of EUROFER97 [4].

Primary displacement damage rate					
	IFMIF-DONES beam energy [MeV]		DEMO FW		
	25	40	DCLL	WCLL	HCPB
NRT_dpa fpy^{-1}	6.65	21.02	11.79	11.32	8.24

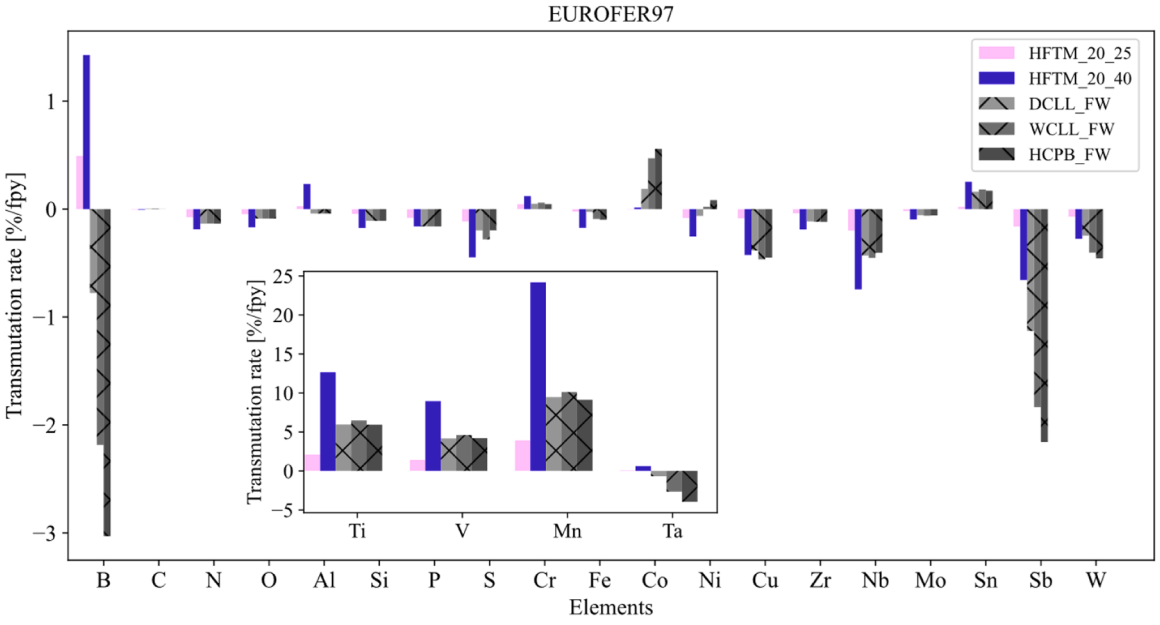

Fig. 3. Transmutation rates in [% fpy^{-1}] of EUROFER97 under irradiation in specimen A at different beam energies in IFMIF-DONES; together with the transmutation rates in the first wall of the fusion power reactors with DCLL, WCLL, and HCPB blankets, Ti, V, Mn and Ta are presented in a different scale.

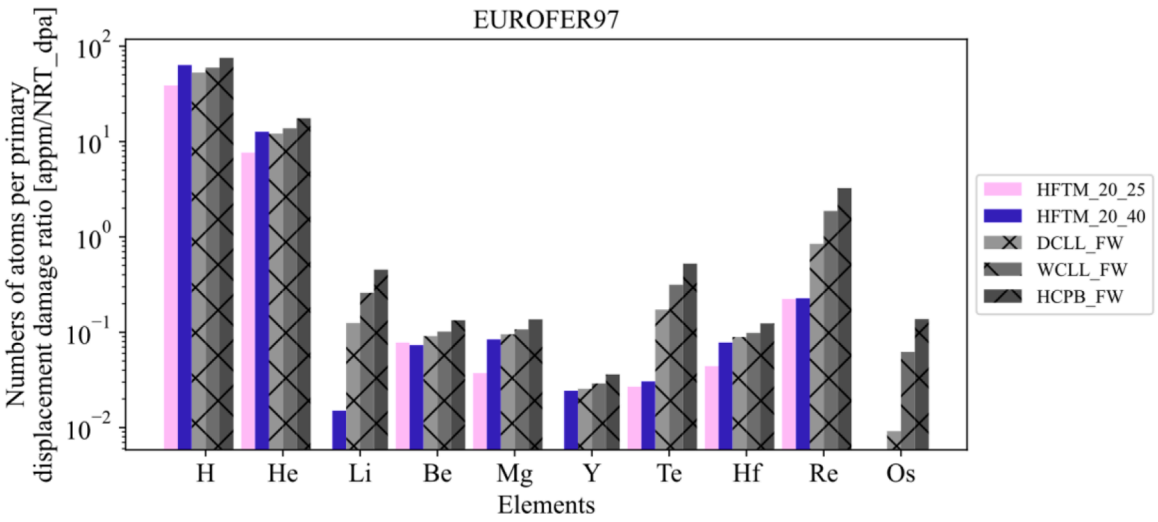

Fig. 4. Numbers of atoms in [appm NRT_dpa^{-1}] of the new elements generated in the EUROFER97 under irradiation in specimen A at different beam energies in IFMIF-DONES and in the first wall of the fusion power reactors with DCLL, WCLL and HCPB blankets.

Table 3
EUROFER97 specification [44], initial (Table 1) and final composition in [wt%]. Two different cases are considered, depending on the IFMIF-DONES beam energy. Three different cases are considered, depending on the DEMO design.

Element	Specif [33,51]	Initial Comp [43]	HFTM _20_25	HFTM _20_40	DCLL _FW	WCLL _FW	HCPB _FW
H			$4.88\bullet10^{-4}$	$2.58\bullet10^{-3}$	$1.15\bullet10^{-3}$	$1.24\bullet10^{-3}$	$1.14\bullet10^{-3}$
He			$3.66\bullet10^{-4}$	$1.91\bullet10^{-3}$	$1.03\bullet10^{-3}$	$1.12\bullet10^{-3}$	$1.04\bullet10^{-3}$
Li				$3.98\bullet10^{-6}$	$1.85\bullet10^{-5}$	$3.70\bullet10^{-5}$	$4.69\bullet10^{-5}$
Be			$8.40\bullet10^{-6}$	$2.49\bullet10^{-5}$	$1.74\bullet10^{-5}$	$1.86\bullet10^{-5}$	$1.78\bullet10^{-5}$
B	$1\bullet10^{-3}$	$2.0\bullet10^{-3}$	$2.01\bullet10^{-3}$	$2.03\bullet10^{-3}$	$1.98\bullet10^{-3}$	$1.96\bullet10^{-3}$	$1.94\bullet10^{-3}$
C	$0.9–1.2\bullet10^{-1}$	$1.1\bullet10^{-1}$	$1.10\bullet10^{-1}$	$1.10\bullet10^{-1}$	$1.10\bullet10^{-1}$	$1.10\bullet10^{-1}$	$1.10\bullet10^{-1}$
N	$1.5–4.5\bullet10^{-2}$	$3.0\bullet10^{-2}$	$2.99\bullet10^{-2}$	$2.99\bullet10^{-2}$	$2.99\bullet10^{-2}$	$2.99\bullet10^{-2}$	$2.99\bullet10^{-2}$
O	$1\bullet10^{-2}$	$1.0\bullet10^{-2}$	$9.99\bullet10^{-3}$	$9.98\bullet10^{-3}$	$9.99\bullet10^{-3}$	$9.99\bullet10^{-3}$	$9.99\bullet10^{-3}$
Mg			$1.85\bullet10^{-5}$	$7.91\bullet10^{-5}$	$5.05\bullet10^{-5}$	$5.46\bullet10^{-5}$	$5.06\bullet10^{-5}$
Al	$1\bullet10^{-2}$	$1.0\bullet10^{-2}$	$1.04\bullet10^{-2}$	$1.00\bullet10^{-2}$	$9.99\bullet10^{-3}$	$1.00\bullet10^{-2}$	$1.00\bullet10^{-2}$
Si	$5\bullet10^{-2}$	$5.0\bullet10^{-2}$	$5.37\bullet10^{-2}$	$4.99\bullet10^{-2}$	$4.99\bullet10^{-2}$	$5.00\bullet10^{-2}$	$5.00\bullet10^{-2}$
P	$5\bullet10^{-3}$	$5.0\bullet10^{-3}$	$5.21\bullet10^{-3}$	$4.99\bullet10^{-3}$	$4.99\bullet10^{-3}$	$4.99\bullet10^{-3}$	$5.00\bullet10^{-3}$
S	$5\bullet10^{-3}$	$5.0\bullet10^{-3}$	$5.37\bullet10^{-3}$	$4.98\bullet10^{-3}$	$4.99\bullet10^{-3}$	$4.99\bullet10^{-3}$	$4.99\bullet10^{-3}$
Ti	$1\bullet10^{-2}$	$2.0\bullet10^{-2}$	$2.04\bullet10^{-2}$	$2.26\bullet10^{-2}$	$2.12\bullet10^{-2}$	$2.13\bullet10^{-2}$	$2.12\bullet10^{-2}$
V	$1.5–2.5\ 10^{-1}$	$2.0\bullet10^{-1}$	$2.03\bullet10^{-1}$	$2.18\bullet10^{-1}$	$2.08\bullet10^{-1}$	$2.09\bullet10^{-1}$	$2.09\bullet10^{-1}$
Cr	$8.5–9.5\bullet10^{0}$	$9.0\bullet10^{0}$	$9.01\bullet10^{0}$	$9.02\bullet10^{0}$	$9.01\bullet10^{0}$	$9.01\bullet10^{0}$	$9.01\bullet10^{0}$
Mn	$2–6\bullet10^{-1}$	$4.0\bullet10^{-1}$	$4.16\bullet10^{-1}$	$4.96\bullet10^{-1}$	$4.38\bullet10^{-1}$	$4.40\bullet10^{-1}$	$4.37\bullet10^{-1}$
Fe	$8.7–9.0\bullet10^{1}$	$8.9\bullet10^{1}$	$8.87\bullet10^{1}$	$8.86\bullet10^{1}$	$8.87\bullet10^{1}$	$8.87\bullet10^{1}$	$8.87\bullet10^{1}$
Co	$5\bullet10^{-3}$	$1.0\bullet10^{-2}$	$1.00\bullet10^{-2}$	$1.00\bullet10^{-2}$	$1.00\bullet10^{-2}$	$1.00\bullet10^{-2}$	$1.01\bullet10^{-2}$
Ni	$5\bullet10^{-3}$	$1.0\bullet10^{-2}$	$1.00\bullet10^{-2}$	$9.98\bullet10^{-3}$	$1.00\bullet10^{-2}$	$1.00\bullet10^{-2}$	$1.00\bullet10^{-2}$
Cu	$5\bullet10^{-3}$	$1.0\bullet10^{-2}$	$9.99\bullet10^{-3}$	$9.97\bullet10^{-3}$	$9.96\bullet10^{-3}$	$9.96\bullet10^{-3}$	$9.96\bullet10^{-3}$
Y				$8.17\bullet10^{-5}$	$4.81\bullet10^{-5}$	$5.25\bullet10^{-5}$	$4.76\bullet10^{-5}$
Zr	a	$5.0\bullet10^{-2}$	$5.00\bullet10^{-2}$	$4.99\bullet10^{-2}$	$5.00\bullet10^{-2}$	$5.00\bullet10^{-2}$	$5.00\bullet10^{-2}$
Nb	$1\bullet10^{-3}$	$5.0\bullet10^{-3}$	$4.99\bullet10^{-3}$	$4.97\bullet10^{-3}$	$4.98\bullet10^{-3}$	$4.98\bullet10^{-3}$	$4.98\bullet10^{-3}$
Mo	$5\bullet10^{-3}$	$5.0\bullet10^{-3}$	$5.00\bullet10^{-3}$	$5.00\bullet10^{-3}$	$5.00\bullet10^{-3}$	$5.00\bullet10^{-3}$	$5.00\bullet10^{-3}$
Sn	b	$5.0\bullet10^{-2}$	$5.00\bullet10^{-2}$	$5.02\bullet10^{-2}$	$5.01\bullet10^{-2}$	$5.01\bullet10^{-2}$	$5.01\bullet10^{-2}$
Sb	c	$5.0\bullet10^{-2}$	$4.99\bullet10^{-2}$	$4.97\bullet10^{-2}$	$4.94\bullet10^{-2}$	$4.91\bullet10^{-2}$	$4.90\bullet10^{-2}$
Te			$3.92\bullet10^{-5}$	$1.41\bullet10^{-4}$	$4.48\bullet10^{-4}$	$7.85\bullet10^{-4}$	$9.48\bullet10^{-4}$
Hf			$9.50\bullet10^{-5}$	$5.29\bullet10^{-4}$	$3.40\bullet10^{-4}$	$3.61\bullet10^{-4}$	$3.30\bullet10^{-4}$
Ta	$5–9\bullet10^{-2}$	$1.2\bullet10^{-1}$	$1.20\bullet10^{-1}$	$1.21\bullet10^{-1}$	$1.19\bullet10^{-1}$	$1.17\bullet10^{-1}$	$1.15\bullet10^{-1}$
W	$1–2\bullet10^{0}$	$1.1\bullet10^{0}$	$1.10\bullet10^{0}$	$1.10\bullet10^{0}$	$1.10\bullet10^{0}$	$1.10\bullet10^{0}$	$1.10\bullet10^{0}$
Re			$4.97\bullet10^{-4}$	$1.59\bullet10^{-3}$	$3.32\bullet10^{-3}$	$7.07\bullet10^{-3}$	$8.97\bullet10^{-3}$
Os					$3.60\bullet10^{-5}$	$2.37\bullet10^{-4}$	$3.81\bullet10^{-4}$
$a+b+c=5\bullet10^{-2}$							

decrease over time rather than increase. Among the newly generated elements, H and He are particularly notable due to their significant proportions. However, some solid second phases could emerge from the transmutation inventory [50]. The transmutation data obtained suit with the data presented in [50], considering 21.02 NRT_dpa fpy^{-1} and 40 MeV beam energy in the IFMIF-DONES case.

3.2. Tungsten

The element initially present in the W composition with the highest production during the irradiation is Ta, showing up to two orders of magnitude increase per dpa. Fig. 5 shows these results. However, it should be noted that the initial concentration of Ta is very low, from $2\bullet10^{-3}$ wt%, it increases up to $1.35\bullet10^{1}$ wt% in the HFTM_20_40 case (Table 5).

Moreover, Fig. 5 shows the elements generated during the irradiation

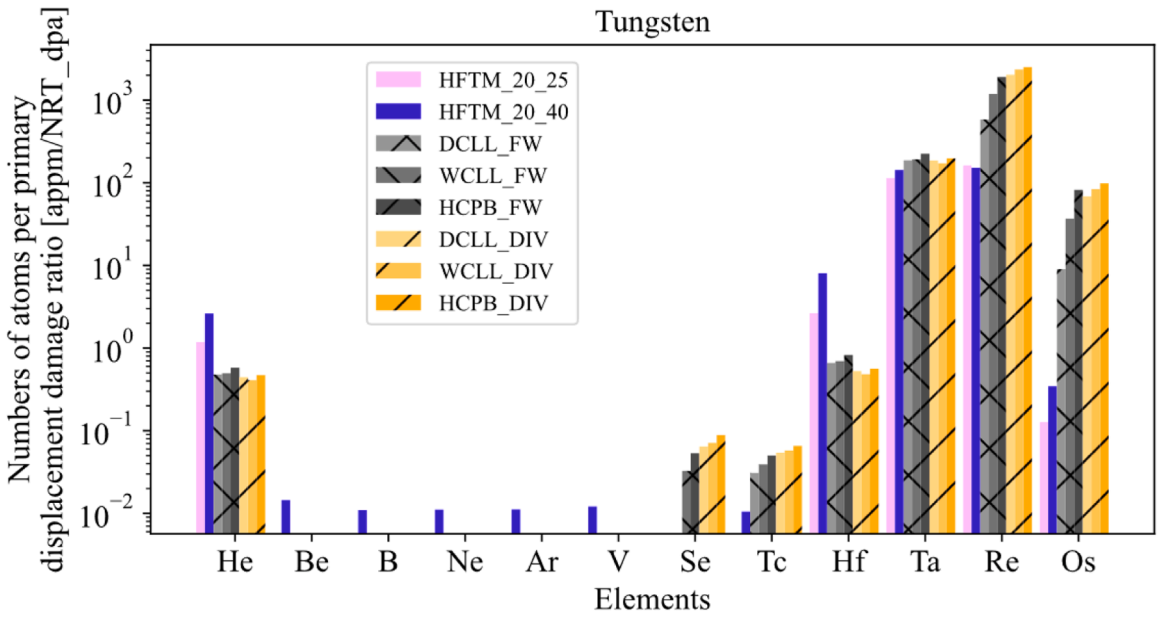

Fig. 5. Numbers of atoms in [appm NRT_dpa^{-1}] of the new elements generated in W under irradiation in specimen A at different beam energies in IFMIF-DONES and in the first wall and in the divertor of the fusion power reactors with DCLL, WCLL and HCPB blankets. The initial composition of Ta is 20.27 appm.

that are not present in the initial composition of W, to obtain the ratio referring the primary displacement damage rate has been used the values presented in Table 4. Be, B, Ne, Ar and V are elements that are only generated in IFMIF-DONES when using an energy of 40 MeV, while Se is only generated in the DEMO cases. The values obtained for DEMO FW and DIV agree regardless of the DEMO design, except for Re and Os cases, moreover, it should be noted that IFMIF-DONES does not reach those values. Taking into account a 9.58 NRT_dpa fpy^{-1} for IFMIF-DONES at 40 MeV beam energy, the transmutation data presented matches well with values obtained in previous works [50].

Re and Os are the main focus as they have a significant influence on the behaviour of W after irradiation. Fig. 7 shows the Re and Os isotopes production in [appm NRT_dpa^{-1}]. Fig. 5 and Fig. 7 show that Re and Os production is higher in DEMO than in IFMIF-DONES. To understand this, we used the ACAB code to assess the formation of ^{188}Os from ^{186}W. The ACAB code indicates that all the pathways to generate ^{188}Os start with the neutron capture of ^{186}W. Moreover, this code gives us the collapsed cross section with the neutron spectrum, obtaining that in DEMO the cross section is two orders of magnitude higher than in IFMIF-DONES, due to the higher neutron capture cross section of ^{186}W for thermal neutrons (Fig. 6). Therefore, these data can explains why more ^{188}Os is generated in DEMO than in IFMIF-DONES.

The production of Re and Os ranges between approximately 4.2–86.1•10^{-2} wt% for Re and 0.02–33.60•10^{-3}wt% for Os (Table 5). In comparison, studies in the literature typically examine W-Re-Os alloys with at least 5 wt% Re and 3 wt% Os [52,57], which are significantly higher than the values obtained here. Therefore, within the 1 fpy considered, the amount of Re and Os produced, up to 8.2 and 0.35•10^{-1} wt% (Table 5), may not be sufficient to significantly affect the properties of W [52,57].

Considering that when Re and Os reach 5 and 3 wt% respectively, W already shows changes in its macroscopic properties, the irradiation time required to reach these values has been analyzed, Re and Os production data were evaluated after 5 and 10 fpy. The analysis focused on two cases: HFTM_20_40 and HCPB_FW, as they present the highest Re and Os values for IFMIF-DONES and DEMO, respectively, at 1 fpy (Table 5). The results, summarised in Table 6, show that the concentrations of Re and Os capable of affecting material properties are reached after 10 years of irradiation in the first wall of HCPB. In contrast, for IFMIF-DONES, these thresholds are not reached even after 10 fpy.

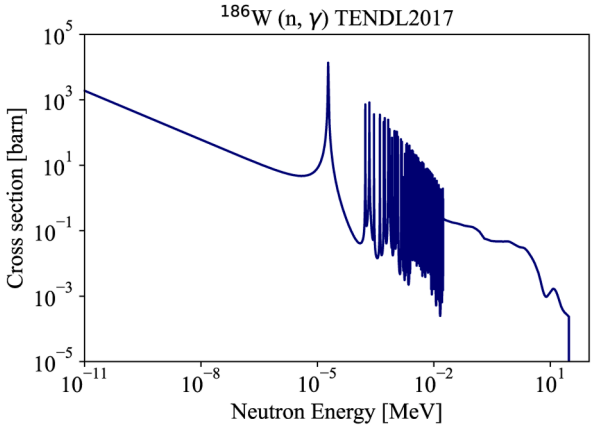

Fig. 6. Cross section ^{186}W(n, γ)^{187}W using TENDL2017 nuclear data library. Both axes are on a logarithmic scale.

Table 4
Primary displacement damage rate in [NRT_dpa fpy^{-1}]in the chosen specimen in IFMIF-DONES and in the first wall and divertor of DEMO in the case of W [5].

Primary displacement damage rate								
	IFMIF-DONES beam energy		DEMO					
			FW			DIV		
	25	40	DCLL	WCLL	HCPB	DCLL	WCLL	HCPB
NRT_dpa fpy^{-1}	2.77	9.58	5.12	4.96	4.21	2.19	2.35	2.19

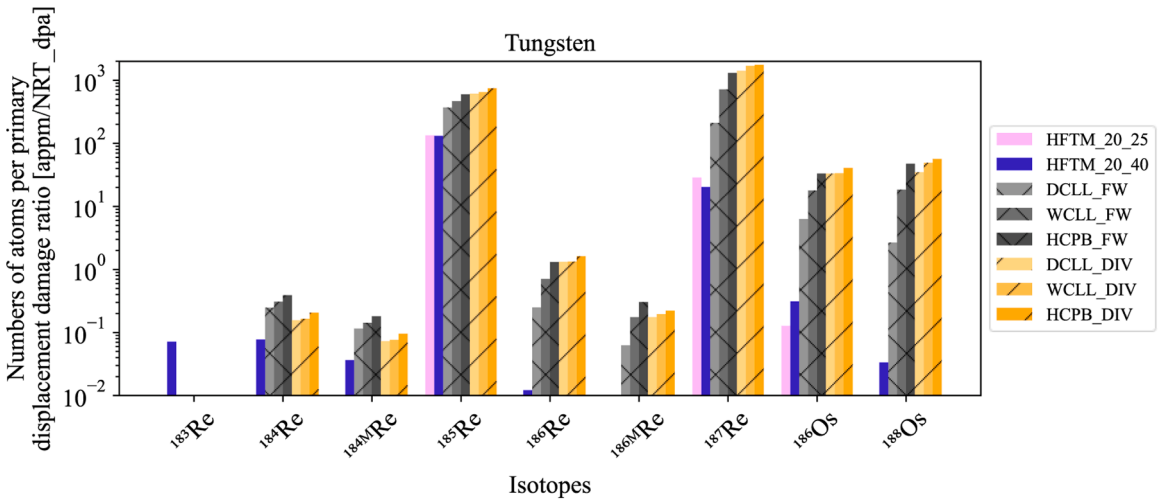

Fig. 7. Numbers of atoms in [appm NRT_dpa^{-1}] of Re and Os isotopes generated in W under irradiation in specimen A at different beam energies in IFMIF-DONES and in the first wall and in the divertor of the fusion power reactors with DCLL, WCLL and HCPB blankets.

Table 5
Weight percent [wt%] Ta, W, Re and Os before and after 1 fpy of the W irradiation using the codes ACAB and TENDL2017 library.

Initial and final composition of TA, W, Re and Os in W									
Elem.	Initial comp.	HFTM _20_25	HFTM _20_40	DCLL _FW	WCLL _FW	HCPB _FW	DCLL _DIV	WCLL _DIV	HCPB _DIV
Ta	$2\bullet10^{-3}$	$3.1\bullet10^{-2}$	$1.35\bullet10^{-1}$	$9.5\bullet10^{-2}$	$9.40\bullet10^{-2}$	$9.30\bullet10^{-2}$	$4.00\bullet10^{-2}$	$4.00\bullet10^{-2}$	$4.30\bullet10^{-2}$
W	$9.99\bullet10^{1}$	$9.99\bullet10^{1}$	$9.97\bullet10^{1}$	$9.96\bullet10^{1}$	$9.93\bullet10^{1}$	$9.90\bullet10^{1}$	$9.95\bullet10^{1}$	$9.93\bullet10^{1}$	$9.93\bullet10^{1}$
Re	–	$5.00\bullet10^{-2}$	$1.50\bullet10^{-1}$	$3.00\bullet10^{-1}$	$6.00\bullet10^{-1}$	$8.20\bullet10^{-1}$	$4.50\bullet10^{-1}$	$5.60\bullet10^{-1}$	$5.60\bullet10^{-1}$
Os	–	$3.59\bullet10^{-5}$	$3.35\bullet10^{-4}$	$4.69\bullet10^{-3}$	$1.90\bullet10^{-2}$	$3.50\bullet10^{-2}$	$1.50\bullet10^{-2}$	$2.00\bullet10^{-2}$	$2.20\bullet10^{-2}$

Table 6
Weight percent [wt%] of Re and Os after different times of irradiation for the case of the HFTM_20_40 and HCPB_FW.

Weight percent [wt%] after irradiation				
		fpy		
		1	5	10
HFTM_20_40	Re	$1.47\bullet10^{-1}$	$8.94\bullet10^{-1}$	$1.74\bullet10^{0}$
	Os	$3.00\bullet10^{-4}$	$1.20\bullet10^{-2}$	$4.70\bullet10^{-2}$
HCPB_FW	Re	$8.16\bullet10^{-1}$	$3.57\bullet10^{0}$	$5.53\bullet10^{0}$
	Os	$3.50\bullet10^{-2}$	$9.29\bullet10^{-1}$	$3.13\bullet10^{0}$

3.3. CuCrZr alloy

In this section are presented the transmutation calculations for the CuCrZr alloy. Fig. 8 shows the elements generated during the irradiation, and the elements initially present in the alloy that present the highest transmutation rates (Co, Ni, and Zn) in [appm NRT_dpa^{-1}]. The primary displacement damage rates obtained for the different IFMIF-DONES cases and DEMO designs [5] are shown in Table 7.

Table 8 summarises the initial composition of the Cu in the alloy used and the proportions after irradiation in the different cases considered for Co, Ni, and Zn.

4. Discussion

In the EUROFER97 case, the transmutation data agree with the ranges specified for this material (Table 3). The most relevant changes are the gas production, H and He. In the case of He, the amount produced is around 10^2 appm fpy^{-1}. This is particularly important since some experiments indicate that when He concentration reaches $5\bullet10^2$ appm, hardening increases [53] and with $5\bullet10^3$ appm, brittleness increases significantly [54,55]. Fig. 3 shows that Mn presents a higher production in IFMIF-DONES than in DEMO. Mn isotopes produced during the irradiation are ^{53}Mn and ^{54}Mn; both isotopes are unstable with long half-lives. These isotopes are generated principally via (n, p) and (n, np) reactions, which require a threshold energy to occur. The IFMIF-DONES facility exhibits a higher neutron flux at higher neutron energies. This is likely the key factor accounting for the differences between facilities. Moreover, this difference in the neutron spectra could explain the Os production. This element comes from neutron capture reactions of W, and its cross sections are higher at lower neutron energies.

On the other hand, Y is generated in greater quantities in IFMIF-DONES than in DEMO, and only at an incident energy of 40 MeV. This is because the production of ^{89}Y is mainly due to ^{90}Zr from the threshold reaction (n, d), which reaches a cross section value of 1 bar from 10 MeV neutrons. From the primary displacement damage comparison (Table 2) and transmutation data, it can be concluded that a beam energy of 25 MeV does not reach the levels in DEMO, but with a 40 MeV energy, more than expected is generated in DEMO. So, intermediate beam energies seem to be the most attractive.

In the case of W irradiation, Ta, an element initially presents in the composition, shows an increase of up to two orders of magnitude (Fig. 5). However, given its residual nuclear hazard, the recommended maximum content of Ta in the composition is $1\bullet10^{-2}$ wt%, as established in the ITER project [56], a threshold that is exceeded in all cases analysed.

Moreover, during the irradiation, new elements such as Re and Os appear in the composition (Fig. 5), resulting in the transformation of pure W into a W-Re-Os alloy during irradiation [57]. Both elements tend to precipitate, hindering dislocation movement and causing radiation hardening and embrittlement [58–60]. The quantity of Re produced by transmutation specifically increase the ductile to brittle transition temperature (DBTT), making W more susceptible to brittle fracture below certain temperatures [52]. Os also increases hardening and brittleness [61]. Understanding the formation of Re and Os is key. Natural W consists mainly of ^{182}W, ^{183}W, ^{184}W and ^{186}W. In the DEMO case, >50 %

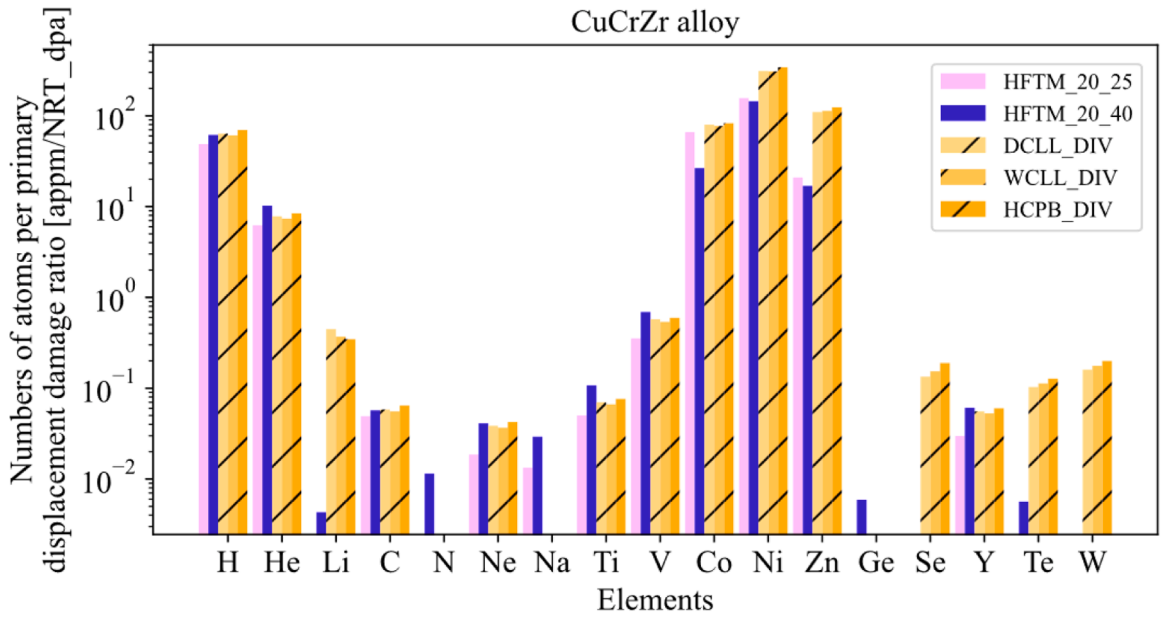

Fig. 8. Numbers of atoms in [appm NRT_dpa^{-1}] of new elements generated in the CuCrZr alloy under irradiation in specimen A at different beam energies in IFMIF-DONES and in the divertor of the fusion power reactors with DCLL, WCLL and HCPB blankets. The initial composition of Co, Ni and Zn is 537.33, 647.43 and 96.87 appm, respectively.

Table 7
Primary displacement damage rate in [NRT_dpa fpy^{-1}]in the chosen specimen in IFMIF-DONES and in the divertor of DEMO in the case of CuCrZr alloy [5].

Primary displacement damage rate					
	IFMIF-DONES beam energy [MeV]		DEMO DIV		
	25	40	DCLL	WCLL	HCPB
NRT_dpa fpy^{-1}	8.79	28.98	7.30	7.55	7.08

of ^{185}W production comes mainly via ^{184}W neutron capture, meanwhile in the case of IFMIF-DONES, >80 % of ^{185}W comes from the ^{186}W via (n, 2n) reactions. On the other hand, ^{185}W decays to ^{185}Re. Further neutron capture can produce ^{186}Re, ^{186m}Re and ^{187}Re. ^{186}Re can decay to ^{186}Os or back to ^{186}W. Although ^{186m}Re and ^{187}Re can also decay to Os isotopes, their contribution is limited by their long half-lives (10^5–10^{10} years). Similarly, ^{186}W can form ^{187}W, which decays to ^{187}Re and finally to Os. ^{188}W can also decay via ^{188}Re to ^{188}Os. Overall, the production of Re and Os is mainly via neutron capture reactions. Fig. 9 shows these

Table 8
Weight percent [wt%] Co, Ni, Cu, and Zn before and after 1 fpy of the CuCrZr alloy irradiation using the codes ACAB and TENDL2017 library.

wt% after 1fpy of irradiation						
Elements	Initial composition	HFTM _20_25	HFTM _20_40	DCLL _DIV	WCLL _DIV	HCPB _DIV
Co	5.00•10^{-2}	5.40•10^{-2}	7.20•10^{-2}	5.40•10^{-2}	5.40•10^{-2}	5.40•10^{-2}
Ni	6.00•10^{-2}	1.32•10^{-1}	4.08•10^{-1}	2.21•10^{-1}	2.27•10^{-1}	2.36•10^{-1}
Cu	9.87•10^{1}	9.84•10^{1}	9.81•10^{1}	9.83•10^{1}	9.83•10^{1}	9.83•10^{1}
Zn	1.00E-02	1.90•10^{-2}	5.00•10^{-2}	8.20•10^{-2}	8.70•10^{-2}	8.90•10^{-2}

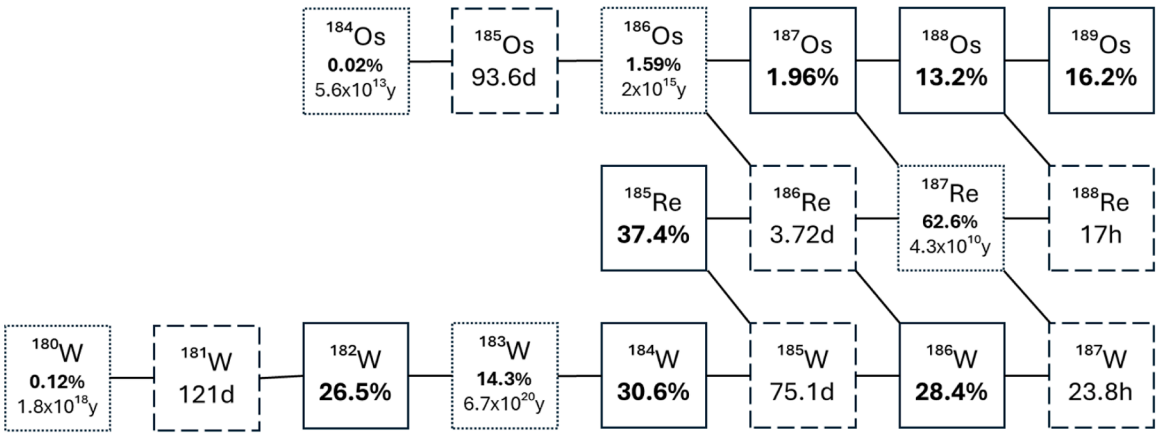

Fig. 9. Os and Re pathway analysis. Stable isotopes are shown in solid-line boxes with their percent abundances indicated in bold. Unstable isotopes appear in dashed-line boxes along with their half-lives, while those that are both unstable and have relatively high abundances and long half-lives are highlighted with dotted-line boxes [62,63].

processes schematically.

In addition, Table 5 shows that the production of Re and Os depends on the DEMO design. In the FW, the DCLL configuration results in lower production compared to the WCLL and HCPB designs. This corresponds to the neutron spectra (Fig. 2) where DCLL has the lowest thermal neutron fluence rate. However, in the case of the divertor, the neutron flux is more uniform, resulting in more consistent Re and Os production across the designs.

The largest contribution to Re and Os production comes from the ^{186}W isotope. Therefore, a potential strategy to mitigate their formation could be to reduce the ^{186}W content in the initial W composition [7]. The results presented here are based on a ^{186}W abundance of 28.34 %. The transmutation data obtained are in good agreement with the results of [7], especially considering the currently lower operating power of DEMO.

From the primary displacement damage rate data presented in Table 4, it can be concluded that an energy of at least 40 MeV is required in IFMIF-DONES to reproduce the displacement damage rates observed in the DEMO FW. For the DIV region, 25 MeV appears to be sufficient. In the case of transmutation, both facilities present a number of atoms per primary displacement damage rate is good agreement.

The generation of new elements during irradiation of CuCrZr alloy (Fig. 8) shows that for the DEMO DIV are similar regardless of the DEMO concept. In the case of the IFMIF-DONES specimen, the numbers of atoms per primary displacement damage ratio is in good agreement regardless the beam energy, but the dpa reached when using the 25 MeV beam energy is three times lower. Se and W are not generated, and Li and Te do not reach DEMO values (only generated at 40 MeV beam energy). On the other hand, N, Na, and Ge are only generated in IFMIF-DONES. H and He are the elements most generated in both facilities. In the case of C all the cases present data in good agreement and in the cases of Ti and V, the number of atoms per primary displacement damage rate is higher when using the nominal beam energy.

The elements initially present in the CuCrZr alloy that show the highest increase are Co, Ni and Zn (Fig. 8). In the cases of Ni and Zn, the values are unattainable for IFMIF-DONES. In the case of Co, the results obtained using a beam energy of 25 MeV align better with expectations than those obtained at the nominal energy of 40 MeV. It is due to the units used, although more cobalt nuclei are generated in the case of 40 MeV, it does not reach the ratio of 3.3 times greater as occurs with primary displacement damage rate. These three elements are just the elements that can drastically change the material thermal conductivity [39,64–67]. The high thermal conductivity of this material is what makes it interesting for use in DEMO, but an increase of Zn, Ni and Co content in the alloy is directly related to the degradation of the thermal conductivity.

Comparing the initial and final composition of the CuCrZr alloy (Table 8), it can be concluded that the three elements present an increase in the weight percent of the material. For the case of Ni, the different DEMO configurations present between 2.1–2.3•10^{-1} wt%, while for the case of IFMIF-DONES, one goes from 1.3•10^{-1} wt% with 25 MeV and 4.1•10^{-1} wt% with 40 MeV. This indicates that, using the lowest energy in IFMIF-DONES, the Ni production is not as high as for DEMO, but using the maximum energy, the value is doubled. In the case of Co, the percentages obtained for DEMO and for IFMIF-DONES with the lowest energy are practically the same, 5.8•10^{-2} wt%, while for the highest energy, it goes up to 7.6•10^{-2} wt%. However, in the case of Zn, the highest values correspond to the DEMO cases, with a value of 8.7•10^{-2} wt%, and the maximum that is reached in IFMIF-DONES is 5.3•10^{-2} wt%.

Focusing only on the primary displacement damage data (Table 7), it can be observed that, from the minimum energy for IFMIF-DONES, 25 MeV, more dpa than expected is achieved for DEMO in all cases. Therefore, using the maximum energy, 40 MeV, in 1 fpy of IFMIF-DONES up to 4 fpy of DEMO can be reproduced. When relating this data to the transmutation results, it can be observed that the trend varies according to the element taken into account. Co, Cu and Zn are the elements that are most generated, and which influence the thermal conductivity of the material. The data for Co in IFMIF-DONES reach those of DEMO, but and in the cases of Ni and Zn they are unattainable.

5. Conclusions

In this study, the transmutation analysis of EUROFER97, W, and CuCrZr alloy in both IFMIF-DONES and DEMO facilities is presented. Two IFMIF-DONES beam energies have been considered to analyse the range of operation of the facility. In general, the number of atoms produced per primary displacement damage ratio are in good agreement independently of the beam energy. However, it is essential to consider that using the lowest beam energy, 25 MeV, the irradiation time must be at least doubled to achieve the same primary displacement damage rate as with the nominal beam energy of 40 MeV.

The results show that in the case of EUROFER97, the transmutation rates are very low and generally within the limits established for this material. The elements to be taken into account are H and He, because they are generated in non-negligible quantities and have a great impact on the mechanical and physical properties of EUROFER97, increasing hardening and brittleness.

In the case of W, the variation in most of its components is very low. Of the materials initially present, Ta is the one that shows the greatest increase, and which has a restricted range due to the activation issue. Among the new elements that will have the greatest influence on the material's properties are Re and Os, increasing hardening or reducing the ductile to brittle transition temperature. Both elements are generated after being irradiated in DEMO and IFMIF-DONES. However, the data achieved in the case of DEMO are much higher. It is also worth noting that the concentrations of Re and Os capable of affecting the material properties are reached after 10 years of irradiation in the first wall of the HCPB concept.

In the case of CuCrZr alloy, the results show that the presence of Co, Ni, and Zn, three of the elements that have the greatest influence on the thermal properties of this alloy, is increased. The magnitudes obtained in both facilities are equivalent.

Based on the present work, this study could be extended by exploring different IFMIF-DONES beam energies and different positions within the HFTM. This extension would help to identify the most effective configuration for each irradiated material, improving the applicability of the current results.

Therefore, after studying three different materials in DEMO and IFMIF-DONES facilities, it can be concluded that the IFMIF-DONES facility can give representative data of what will be obtained later in DEMO.

CRediT authorship contribution statement

Irene Álvarez: Writing – review & editing, Writing – original draft, Validation, Software, Methodology. **Marta Anguiano:** Writing – review & editing, Writing – original draft, Validation, Supervision, Project administration, Methodology, Investigation, Funding acquisition. **Fernando Mota:** Writing – review & editing, Writing – original draft, Validation, Supervision, Software, Methodology, Funding acquisition, Conceptualization. **Rebeca Hernández:** Writing – review & editing, Writing – original draft, Supervision, Resources. **Marta Serrano:** Writing – review & editing, Supervision, Resources. **David Sosa:** Writing – review & editing, Resources. **Iole Palermo:** Writing – review & editing, Resources. **Edgar Leon-Gutierrez:** Writing – review & editing, Resources. **Simone Noce:** Writing – review & editing, Resources. **Fabio Moro:** Writing – review & editing, Resources. **Frederik Arbeiter:** Writing – review & editing, Resources. **Yuefeng Qiu:** Writing – review & editing, Supervision, Resources. **Jin Hun Park:** Writing – review & editing, Resources. **Ángel Ibarra:** Writing – review & editing, Conceptualization.

Declaration of competing interest

The authors declare that they have no known competing financial interests or personal relationships that could have appeared to influence the work reported in this paper.

Acknowledgments

This work has been supported by the European Union's FEDER program, IFMIF-DONES Junta de Andalucia's program at the Universidad de Granada, by MCIN/AEI/10.13039/501100011033/FEDER, UE (PID2022–137543NB-I00) and has been carried out within the framework of the EUROfusion Consortium, funded by the European Union via the Euratom Research and Training Programme (Grant Agreement No 101052200 — EUROfusion). Views and opinions expressed are however, those of the author(s) only and do not necessarily reflect those of the European Union or the European Commission. Neither the European Union nor the European Commission can be held responsible for them. Funding for open access charge: Universidad de Granada / CBUA

Data availability

Data will be made available on request.

References

[1] D. Bernardi, F. Arbeiter, M. Cappelli, U. Fischer, A. García, et al., Towards the EU fusion-oriented neutron source: the preliminary engineering design of IFMIF-DONES, Fusion Eng. Des. 146 (2019) 261–268.
[2] Angel Ibarra, et al., DONES performance, experimental capabilities and perspectives', Nucl. Fusion (2025) https://doi.org/10.1088/1741-4326/adcd86 in press.
[3] I. Álvarez, M. Anguiano, F. Mota, R. Hernández, Y. Qiu, Neutronic assessment of the IFMIF-DONES HFTM specimen stack distribution, Fusion Eng. Des. 200 (2024) 114212, https://doi.org/10.1016/j.fusengdes.2024.114212. Mar.
[4] I. Álvarez, et al., Comparative analysis of neutronic features for various specimen payload configurations within the IFMIF-DONES HFTM, Fusion Eng. Des. 210 (2025) 114729, https://doi.org/10.1016/j.fusengdes.2024.114729. Jan.
[5] I. Álvarez, et al., Assessment of the possibility of irradiating tungsten and Cu-alloys in IFMIF-DONES using a realistic specimens configuration, Nucl. Fusion 65 (2) (2025) 026058, https://doi.org/10.1088/1741-4326/ada6da. Feb.
[6] M.R. Gilbert, S.L. Dudarev, S. Zheng, L.W. Packer, J.-Ch. Sublet, An integrated model for materials in a fusion power plant: transmutation, gas production, and helium embrittlement under neutron irradiation, Nucl. Fusion 52 (8) (2012) 083019, https://doi.org/10.1088/0029-5515/52/8/083019. Aug.
[7] M.R. Gilbert, J.-Ch. Sublet, Neutron-induced transmutation effects in W and W-alloys in a fusion environment, Nucl. Fusion 51 (4) (2011) 043005, https://doi.org/10.1088/0029-5515/51/4/043005. Apr.
[8] G. Pintsuk, et al., European materials development: results and perspective, Fusion Eng. Des. 146 (2019), https://doi.org/10.1016/j.fusengdes.2019.02.063.
[9] Y. Qiu, M. Ansorge, I. Álvarez, K. Ambrožič, T. Berry, et al., Overview of recent advancements in IFMIF-DONES neutronics activities, Fusion Eng. Des. 201 (2024) 114242, https://doi.org/10.1016/j.fusengdes.2024.114242. ISSN 0920-3796.
[10] I. Fernández-Berceruelo, I. Palermo, F.R. Urgorri, A. García, D. Rapisarda, et al., Alternatives for upgrading the EU DCLL breeding blanket from MMS to SMS, Fusion Eng. Des. 167 (2021), https://doi.org/10.1016/j.fusengdes.2021.112380.
[11] D. Rapisarda, I. Fernández-Berceruelo, A. García, J.M. García, B. Garcinuño, et al., The European Dual Coolant lithium lead breeding blanket for DEMO: status and perspectives, Nucl. Fusion 61 (2021), https://doi.org/10.1088/1741-4326/ac26a1.
[12] P. Arena, A. Del Nevo, F. Moro, S. Noce, R. Mozzillo, et al., The DEMO water-cooled lead–lithium breeding blanket: design status at the end of the pre-conceptual design phase, Appl. Sci. 11 (2021), https://doi.org/10.3390/app112411592.
[13] F. Moro, P. Arena, I. Catanzaro, A. Colangeli, A. Del Nevo, et al., Nuclear performances of the water-cooled lithium lead DEMO reactor: neutronic analysis on a fully heterogeneous model, Fusion Eng. Des. 168 (2021) 112514, https://doi.org/10.1016/j.fusengdes.2021.112514. ISSN 0920-3796.
[14] S. Noce, et al., Neutronics assessment of the spatial distributions of the nuclear loads on the DEMO divertor ITER-like targets: comparison between the WCLL and HCPB blanket, Appl. Sci. 13 (3) (2023) 1715, https://doi.org/10.3390/app13031715.
[15] I. Palermo, F.A. Hernández, P. Pereslavtsev, D. Rapisarda, G. Zhou, Shielding design optimization of the helium-cooled pebble bed breeding blanket for the EU DEMO fusion reactor, Energies 15 (2022), https://doi.org/10.3390/en15155734.
[16] G. Zhou, F.A. Hernández, P. Pereslavtsev, B. Kiss, A. Retheesh, et al., The European DEMO helium cooled pebble bed breeding blanket: design status at the conclusion of the pre-concept design phase, Energies 16 (2023), https://doi.org/10.3390/en16145377.
[17] G. Zhou, J. Aktaa, D. Alonso, L.V. Boccaccini, I. Cristescu, et al., "Design update of the European DEMO helium cooled pebble bed breeding blanket" (CBBI-21 2023), Granada, Spanien, 19.–20. Oktober 2023. https://publikationen.bibliothek.kit.edu/1000165661.
[18] A. Konobeyev, Yu. Korovin, P. Pereslavtsev, U. Fischer, U. Von Möllendorff, Development of methods for calculation of deuteron-lithium and neutron-lithium cross sections for energies up to 50 MeV, Nucl. Sci. Eng. 139 (2001) 1–23.
[19] 'FENDL-3.1d: fusion evaluated nuclear data library ver.3.1d', Accessed: Oct. 09, 2024. [Online]. Available: https://www-nds.iaea.org/fendl/.
[20] A. Serikov, 'MCNP model "mdl9.2.8" with updates of the IFMIF-DONES Test Cell components', 2023, 1.1. Accessed: Feb. 07, 2025. [Online]. Available: https://idm.euro-fusion.org/default.aspx?uid=2QQ9CC.
[21] I. Álvarez, M. Anguiano, F. Mota, Y. Qiu, and F. Arbeiter, '2023_Neutronics_TC_mdl9.2.8_CLC.V2.0 (2PRQXX)', 2023, 1.0. Accessed: Feb. 07, 2025. [Online]. Available: https://idm.euro-fusion.org/default.aspx?uid=2PRQXX.
[22] EUROfusion, 'European research roadmap to the realisation of fusion energy', 2018. doi: https://euro-fusion.org/wp-content/uploads/2022/10/2018_Research_roadmap_long_version_01.pdf.
[23] B. van der Schaaf, et al., The development of EUROFER reduced activation steel, Fusion Eng. Des. 69 (2003), https://doi.org/10.1016/S0920-3796(03)00337-5. Sept.
[24] F. Tavassoli, Eurofer steel, development to full code qualification, Procedia Eng. 55 (2013), https://doi.org/10.1016/j.proeng.2013.03.258.
[25] E. Lucon, et al., The European effort towards the development of a demo structural material: irradiation behaviour of the European reference RAFM steel EUROFER, Fusion Eng. Des. 81 (2006) 917, https://doi.org/10.1016/j.fusengdes.2005.08.044. Feb.
[26] A. Bhattacharya, et al., Irradiation damage concurrent challenges with RAFM and ODS steels for fusion reactor first-wall/blanket: a review, J. Phys. Energy 4 (2022), https://doi.org/10.1088/2515-7655/ac6f7f.
[27] R. Neu, et al., Advanced tungsten materials for plasma-facing components of DEMO and fusion power plants, Fusion Eng. Des. 109 (2016) 1046, https://doi.org/10.1016/j.fusengdes.2016.01.027. Nov.
[28] J.W. Coenen, et al., Materials for DEMO and reactor applications—boundary conditions and new concepts, Phys. Scr. (2016) 2016, https://doi.org/10.1088/0031-8949/2016/T167/014002.
[29] J.H. You, et al., Conceptual design studies for the European DEMO divertor: rationale and first results, Fusion Eng. Des. 109 (2016) 1598, https://doi.org/10.1016/j.fusengdes.2015.11.012. Nov.
[30] S.J. Zinkle, Applicability of copper alloys for DEMO high heat flux components, Phys. Scr. 2016 (2016), https://doi.org/10.1088/0031-8949/2015/T167/014004.
[31] G. Pintsuk, et al., Materials for in-vessel components, Fusion Eng. Des. 174 (2022) 112994, https://doi.org/10.1016/j.fusengdes.2021.112994. Jan.
[32] K. Mergia, N. Boukos, Structural, thermal, electrical and magnetic properties of Eurofer 97 steel, J. Nucl. Mater. 373 (1–3) (2008) 1–8, https://doi.org/10.1016/j.jnucmat.2007.03.267. Feb.
[33] E. Gaganidze, F. Gillemot, I. Szenthe, M. Gorley, M. Rieth, E. Diegele, Development of EUROFER97 database and material property handbook, Fusion Eng. Des. 135 (2018) 9–14, https://doi.org/10.1016/j.fusengdes.2018.06.027. Oct.
[34] R.G. Abernethy, Predicting the performance of tungsten in a fusion environment: a literature review, Mater. Sci. Technol. 33 (2017), https://doi.org/10.1080/02670836.2016.118526. March.
[35] J. Knaster, A. Moeslang, T. Muroga, Materials research for fusion, Nat. Phys. 12 (5) (2016) 424–434, https://doi.org/10.1038/nphys3735. May.
[36] C. Deng, et al., Manufacture of thick VPS W coatings on relatively large CuZrCr substrate and its steady high heat load performance, J. Nucl. Mater. 455 (1–3) (2014) 145–150, https://doi.org/10.1016/j.jnucmat.2014.05.029. Dec.
[37] K. Zhang, E. Gaganidze, M. Gorley, Development of the material property handbook and database of CuCrZr, Fusion Eng. Des. 144 (2019) 148, https://doi.org/10.1016/j.fusengdes.2019.04.094. Jul.
[38] J.H. You, et al., Divertor of the European DEMO: engineering and technologies for power exhaust, Fusion Eng. Desing 175 (2022) 113010, https://doi.org/10.1016/j.fusengdes.2022.113010. Feb.
[39] S.A. Fabritsiev, S.J. Zinkle, B.N. Singh, Evaluation of copper alloys for fusion reactor divertor and first wall components, J. Nucl. Mater. 233–237 (1996) 127–137, https://doi.org/10.1016/S0022-3115(96)00091-8. Oct.
[40] V.R. Barabash, G.M. Kalinin, S.A. Fabritsiev, S.J. Zinkle, Specification of CuCrZr alloy properties after various thermo-mechanical treatments and design allowables including neutron irradiation effects, J. Nucl. Mater. 417 (1–3) (2011) 904–907, https://doi.org/10.1016/j.jnucmat.2010.12.158. Oct.
[41] A. Hernández-Pérez, M. Eddahbi, M.A. Monge, A. Muñoz, B. Savoini, Microstructure and mechanical properties of an ITER-grade Cu–Cr–Zr alloy processed by equal channel angular pressing, Fusion Eng. Des. 98–99 (2015) 1978–1981, https://doi.org/10.1016/j.fusengdes.2015.06.180. Oct.
[42] F. Romanelli, 'A roadmap to the realisation of fusion energy', 2012. Accessed: Feb. 06, 2025. [Online]. Available: www.eurofusion.org/wpcms/wp-content/uploads/2013/01/JG12.356-web.pdf.
[43] U. Fischer and Y. Qiu, 'Material compositions for PPPT neutronics and activation analyses, EUROfusion IDM EFDA_2MM3A6 v1.2.' 2020, Accessed: Feb. 03, 2025. [Online]. Available: https://idm.euro-fusion.org/default.aspx?uid=2MM3A6.
[44] "ITER material property handbook (ITER Document No. G74 MA16 File: ITER-AK02-1100)," 2004.

[45] J. Sanz, O. Cabellos, and N. García-Herranz, 'NEA-1839 ACAB-2008. ACAB-2008, ACtivation ABacus code'. 2008 Accessed: Feb. 03, 2025. [Online]. Available: https://www.oecd-nea.org/tools/abstract/detail/nea-1839.
[46] 'TENDL-2017 library'. 2017 Accessed: Feb. 03, 2025. [Online]. Available: https://www-nds.iaea.org/public/download-endf/TENDL-2017/Original/TENDL-2017.htm.
[47] M.J. Norgett, M.T. Robinson, I.M. Torrens, A proposed method of calculating displacement dose rates, Nucl. Eng. Des. 33 (1975) 50–54, https://doi.org/10.1016/0029-5493(75)90035-7.
[48] C.J. Werner et al., 'MCNP Version 6.2 release notes', United States, 2018. doi:10.2172/1419730.
[49] A.J.M. Plompen, et al., 'The joint evaluated fission and fusion nuclear data library, JEFF-3.3′, Eur. Phys. J. A 56 (7) (2020) 181, https://doi.org/10.1140/epja/s10050-020-00141-9. Jul.
[50] J. Marian, et al., Computational materials assessment of the D/Li-stripping neutron source as a prototypical facility for fusion materials testing, Curr. Opin. Solid State Mater. Sci. 38 (2025) 101231, https://doi.org/10.1016/j.cossms.2025.101231.
[51] P. Fernandez, A.M. Lancha, J. Lapena, M. Serrano, M. Hernandez-Mayoral, and M (Spain) de investigaciones energeticas medioambientales y tecnologicas (CIEMAT), 'reduced activation ferritic/martensitic steel eurofer 97 as possible structural material for fusion devices. Metallurgical characterization on As-received condition and after simulated services conditions', Jan. 2004. Accessed: Nov. 28, 2024. [Online]. Available: https://inis.iaea.org/records/dmghx-tg654#page=32.11.
[52] A. Hasegawa, M. Fukuda, T. Tanno, S. Nogami, Neutron irradiation behavior of tungsten, Mater. Trans. 54 (4) (2013) 466–471, https://doi.org/10.2320/matertrans.MG201208.
[53] M. Roldán, et al., Effect of helium implantation on mechanical properties of EUROFER97 evaluated by nanoindentation, J. Nucl. Mater. 448 (2014) 301–309, https://doi.org/10.1016/j.jnucmat.2014.02.020. May.
[54] P. Jung, J. Henry, J. Chen, J.-C. Brachet, Effect of implanted helium on tensile properties and hardness of 9 % Cr martensitic stainless steels, J. Nucl. Mater. 318 (2003) 241–248, https://doi.org/10.1016/S0022-3115(03)00014-X. May.
[55] J. Henry, M.-H. Mathon, P. Jung, Microstructural analysis of 9 % Cr martensitic steels containing 0.5 at.% helium, J. Nucl. Mater. 318 (2003) 249–259, https://doi.org/10.1016/S0022-3115(03)00118-1. May.
[56] F. Mota, et al., Neutron shielding assessment for the remote handling lower port rack of ITER, Fusion Eng. Des. 135 (2018) 50–58, https://doi.org/10.1016/j.fusengdes.2018.06.023. Oct.
[57] J.-C. He, A. Hasegawa, M. Fujiwara, M. Satou, T. Shishido, K. Abe, Fabrication and characterization of W-re-Os alloys for studying transmutation effects of W in fusion reactors, Mater. Trans. 45 (8) (2004) 2657–2660.
[58] T. Suzudo, M. Yamaguchi, A. Hasegawa, Migration of rhenium and osmium interstitials in tungsten, J. Nucl. Mater. 467 (2015) 418–423, https://doi.org/10.1016/j.jnucmat.2015.05.051. Dec.
[59] A. Hasegawa, T. Tanno, S. Nogami, M. Satou, Property change mechanism in tungsten under neutron irradiation in various reactors, J. Nucl. Mater. 417 (1–3) (2011) 491–494, https://doi.org/10.1016/j.jnucmat.2010.12.114. Oct.
[60] Y. Qian, M.R. Gilbert, L. Dezerald, D. Cereceda, Using first-principles calculations to predict the mechanical properties of transmuting tungsten under first wall fusion power-plant conditions, J. Phys. 33 (34) (2021) 345901, https://doi.org/10.1088/1361-648X/ac08b8. Aug.
[61] I. Smid, M. Akiba, G. Vieider, L. Plöchl, Development of tungsten armor and bonding to copper for plasma-interactive components, J. Nucl. Mater. 258–263 (1998) 160–172, https://doi.org/10.1016/S0022-3115(98)00358-4. Oct.
[62] NIST National Institute of Standards and Technology, 'Atomic weights and isotopic compositions'. Accessed: Feb. 20, 2025. [Online]. Available: https://physics.nist.gov/cgi-bin/Compositions/stand_alone.pl?ele=W.
[63] IAEA, 'Live chart of nuclides'. Accessed: Mar. 27, 2024. [Online]. Available: https://www-nds.iaea.org/relnsd/vcharthtml/VChartHTML.html.
[64] S.A. Fabritsiev, et al., Effect of irradiation temperature and dose on mechanical properties and fracture characteristics of Cu//SS joints for ITER, J. Nucl. Mater. 386–388 (2009) 824–829, https://doi.org/10.1016/j.jnucmat.2008.12.241. Apr.
[65] G.J. Butterworth, Transmutation and activation effects in high-conductivity copper alloys exposed to a first wall fusion neutron flux, J. Nucl. Mater. 135 (2–3) (1985) 160–172, https://doi.org/10.1016/0022-3115(85)90074-1. Oct.
[66] F.A. Garner, Influence of transmutation and high neutron fluence on materials used in fission-fusion correlation experiments, J. Nucl. Mater. 174 (2–3) (1990) 229–239, https://doi.org/10.1016/0022-3115(90)90237-H. Nov.
[67] F.A. Garner, H.L. Heinisch, R.L. Simons, F.M. Mann, Implications of neutron spectrum and flux differences on fission-fusion correlations at high neutron fluence, Radiat. Eff. Defects Solids 113 (1–3) (1990) 229–255, https://doi.org/10.1080/10420159008213068. Mar.